Antarctic Science 12 (1): 105–116 (2000) © British Antarctic Survey Printed in the United Kingdom

Experimental study on a basanite from the McMurdo Volcanic Group, Antarctica: inference on its mantle source

ANDREA ORLANDO[1*], SANDRO CONTICELLI[1,2], PIETRO ARMIENTI[3] and DANIELE BORRINI[1,4]

[1]*C.N.R., Centro di Studio per la Minerogenesi e la Geochimica Applicata, Via G. La Pira, 4, I-50121 Firenze, Italy*
[2]*Università degli Studi della Basilicata, Via N. Sauro, 85, I-85100, Potenza, Italy*
[3]*Dipartimento di Scienze della Terra, Università degli Studi di Pisa, Via S. Maria 53, I-56100 Pisa, Italy*
[4]*Dipartimento di Scienze della Terra, Università degli Studi di Firenze, Via G. La Pira, 4, I-50121 Firenze, Italy*
**aorlando@geo.unifi.it*

Abstract: Experiments to reconstruct the liquidus curve and establish the phase relationships of a basanite (Mg# = 72) from the McMurdo Volcanic Group, (thought to represent a nearly primary magma) used 1.0–3.0 GPa and 1175–1550°C. The results suggest that this basanite could be generated by partial melting either of a spinel lherzolite (at P = 1.5–2.0 GPa and T = 1390–1490°C) or of a garnet pyroxenite (at P > 3.0 GPa and T > 1550°C) source. Several lines of petrological and geochemical evidence support the latter hypothesis. Moreover, experimental results indicate the presence of mica in the source if it is assumed that the magma lost some water during its ascent to the surface. This is supported by the presence of mica and amphibole-bearing mantle xenoliths hosted in the most primitive volcanic rocks of the McMurdo Volcanic Group. These results and observations suggest that the source of magmas underwent metasomatism prior to partial melting.

Received 12 August 1998, accepted 24 September 1999

Key words: Antarctica, basanite, experimental petrology, McMurdo Volcanic Group, petrogenesis

Introduction

Alkaline to transitional volcanic suites are often related to continental break-up, and their study represents an important tool to disentangle the complex geological processes in this geodynamic setting. Furthermore, the reconstruction of the pressure–temperature conditions of magma generation and evolution helps to better constrain the features of the rifting and to define its passive or active nature.

McMurdo Volcanic Group (MMVG) in Antarctica is a Cainozoic–Recent alkaline volcanic province related to the extension in the Ross Sea and represents one of the widest regions in the world where rifting related magmatism occurs (e.g. Harrington 1958, Kyle & Cole 1974, Tonarini *et al.* 1997). The MMVG overlies continental crust ranging in thickness from 17 to 40 km (Trehu *et al.* 1989), which was stretched and thinned during development of the basins of the Ross Sea, although no evidence of oceanization has been found (Davey & Brancolini 1997). Even if the formation of the basins dates back to Cretaceous time, the earliest evidence of magmatism is a set of shallow level Oligocene (48–38 Ma) alkali-gabbro to syenite stocks, which were exposed in North Victoria Land during the uplift of the Western Rift shoulder in the Transantarctic Mountains (Tonarini *et al.* 1997). Magmatism has continuously accompanied the uplift of the Western Rift shoulder producing modest amounts of alkaline magmas (less than 10^{-3} km^3 yr^{-1} in the last 50 Ma, Armienti *et al.* 1995). The most conspicuous developments of igneous rocks are mainly located along the N–S master faults in a belt between the Transantarctic Mountains and the Ross Sea. There the larger intrusions and central volcanoes lie at the intersections between N–S faults and the regional NW–SE strike-slip faults (Kyle & Cole 1974). This pattern of faulting is considered by Salvini *et al.* (1997) to be the expression of a regional right-lateral, strike-slip motion that is co-linear in the last 55 Ma with deformation belts crossing the Southern Ocean, North Victoria Land and Ross Sea accommodating major transform movements along the Tasman and Balleny fracture zones. In this transtensional context, preferential rise of magma occurs where local crustal extension is possible.

Volcanic rocks of the MMVG range from basanites and alkali basalts to phonolites and trachytes, whereas transitional basalts give rise to peralkaline rhyolites and trachytes (e.g. Goldich *et al.* 1975, Beccaluva *et al.* 1991a, Müller *et al.* 1991). The presence of deep magma chambers in which magmatic evolution occurs is strongly suggested by the frequent occurrence of cumulates in suites of ultramafic inclusions. These include wherlites and pyroxenites which often exhibit widespread evidence of veining by hydrous fluids that induce the formation of hornblendite or kaersutite megacrysts (Beccaluva *et al.* 1991b, Gamble & Kyle 1987, Gamble *et al.* 1988, Hornig & Wörner 1991, Armienti *et al.* 1994). The relative abundance of metasomatism in lithospheric mantle in the area is also shown by veined harzburgite nodules and glass blebs in mantle peridotites (Perinelli *et al.* 1998). Among the alkaline and transitional suites, the most mafic rocks frequently represent compositions eligible to have been in equilibrium with their source (Orlando *et al.* 1997). Namely, a basanite from Malta Plateau (MP24, Fig. 1) exhibits compositional (Mg-# = 72; Ni = 367 ppm) and mineralogical data suggestive of a near "primary" nature suggesting that early crystallization

stages occurred within the ranges of 2.0–2.5 GPa and 1250–1300°C (Orlando *et al.* 1997); its melting relationships have been determined in order to constrain experimentally the nature of the mantle source and to characterize the possible P–T conditions in which liquid segregation occurred. Phase relationships and mineral compositions are also presented.

Experimental and analytical techniques

The starting material was a finely-ground (< 50 μm) natural basanite sample (MP24; Orlando *et al.* 1997). Homogeneity and major and trace element contents were accurately checked using different analytical methods on different splits (Table I).

Experiments were performed in a half-inch piston cylinder apparatus using a salt cell/Pyrex pressure medium with a graphite heater. Pressure was applied using the "hot-piston-out" technique and calibrated at the ferrosilite-fayalite+quartz transition (1.41 GPa and 1000°C; Bohlen *et al.* 1980). A 5% negative pressure correction relative to the nominal pressure was found to be necessary. Temperature was continuously monitored using a $Pt/Pt_{90}Rh_{10}$ thermocouple, without any pressure correction applied to the electromotive force. Temperature calibration was performed on the melting point of Au and error was found to be within ± 5°C. Pt and $Ag_{50}Pd_{50}$ capsules were used. In the case of Pt capsules, experimental durations of near-liquidus runs were kept as short as possible (Table II) in order to minimize Fe-loss through capsule walls (Biggar 1977). Experiments were performed with the natural contents of volatile elements after drying the starting material at 120°C for 12 hours to remove any adsorbed H_2O.

Experimental products were studied by optical methods and X-Ray Difractometry. Subsequently primary minerals and glasses were analysed with a JEOL JXA-8600 electron microprobe using an accelerating voltage of 15 kV, a beam current of 10 nA, and counting times ranging from 20 to 40 seconds. Data were corrected for the matrix effect using the

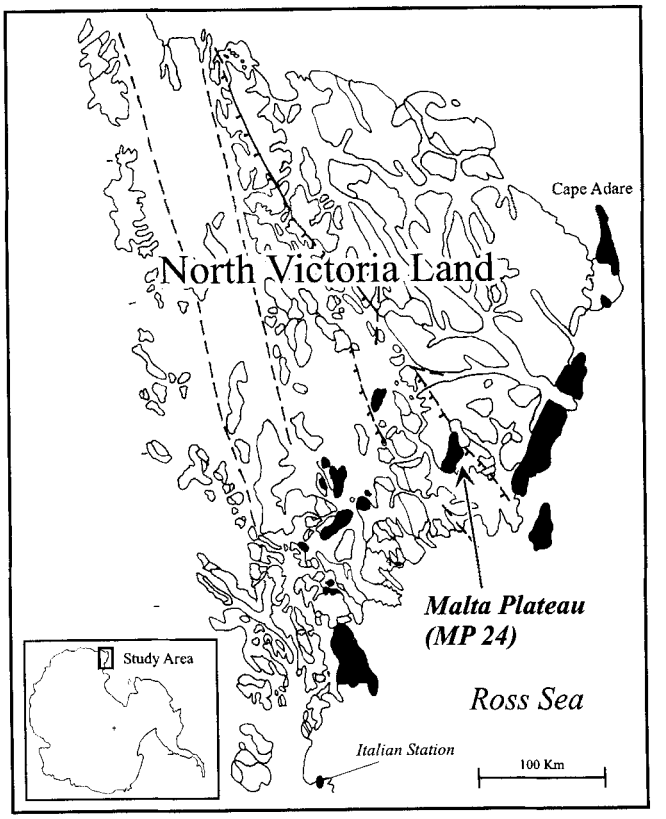

Fig. 1. Volcanic rocks of the MMVG (in black) from North Victoria Land. Malta Plateau indicated: sampling locality of the basanite sample MP24 subject of this study. Map modified from Carmignani *et al.* (1989).

Table I. Composition of the starting material (mean of four analyses) used to study melting relationships in the sample MP24.

	wt %	1σ		ppm	1σ	INAA (ppm)		CS analyses (ppm)	
SiO_2	43.7	0.13	V	298	3	Sc	28.5	C	562
TiO_2	2.69	0.04	Cr	773	13	La	42.8	S	33
Al_2O_3	13.8	0.04	Co	58	1	Ce	79		
Fe_2O_3	2.28	0.14	Ni	367	3	Nd	32	CIPW norm	
FeO	8.08	0.05	Cu	82	3	Sm	7.7	*ab*	6.8
MnO	0.17	0.01	Zn	81	0.9	Eu	2.14	*ne*	10.1
MgO	12.6	0.04	Rb	33	1.1	Tb	0.7	*ol*	19.9
CaO	11.2	0.07	Sr	586	4.7	Yb	1.9		
Na_2O	2.96	0.01	Y	22	2	Lu	0.22	Mg-#	72.3
K_2O	1.24	0.02	Zr	202	5	Hf	4.4	CO_2[2]	0.20
P_2O_5	0.48	0.03	Nb	58	1.9	Ta	4.6	H_2O[3]	0.65
LOI[1]	0.85	0.01	Ba	383	7	Th	5.1		
			La	40	1.5				
			Ce	83	1.9				
			Nd	38	2				
			Pb	14	0.7				
			Th	11	0.9				
			U	3	0.8				

Mg-# = 100*[Mg/(Mg+0.85*Fe)] molar, where Fe is total Fe. CIPW norms: *ab* = albite, *ne* = nepheline *ol* = olivine. INAA after Poli *et al.* (1977).
[1]includes correction for weight gain due to Fe oxidation (Lechler & Desilets 1987), [2]estimated (calculated transforming all C to CO_2) [3]estimated (LOI–CO_2)

https://doi.org/10.1017/S0954102000000134 Published online by Cambridge University Press

Bence & Albee (1968) method. Errors were estimated according to Vaggelli *et al.* (1999).

Experimental results

Experimental conditions and results are listed in Table II; when reversals were performed, durations at the different temperatures are also reported.

Olivine is the liquidus phase between 1.0 and 1.5 GPa, being replaced by clinopyroxene at higher P. Phase relations (Fig. 2a) show that clinopyroxene is present in the whole P–T range, apart from the portion where olivine is the liquidus phase. At P higher than 2.0 GPa olivine stability field is restricted at low T, whereas spinel is found near the liquidus at P higher than 1.5 GPa. Garnet is stable at high P (2.5 and 3.0 GPa) and its stability field approaches the liquidus with increasing P. Although mica laths (length 5–10 μm) are found at P higher than 1.5 GPa, it is most likely a quenched phase.

Comparison between experimental and calculated liquidus curves using MELTS software package (Ghiorso *et al.* 1994, Ghiorso & Sack 1995) is shown in Fig. 2b. The agreement between the calculated and experimentally determined curves is good for P ranging between 2 and 2.5 GPa, whereas at higher pressures, the differences may be due to experimental uncertainty: these pressures are significantly higher than the calibration pressure. The slight discrepancy observed in the range between 1 and 2 GPa is within 15–20°C. The largest deviation is observed at 1.6 GPa where the experimental liquidus curve is interpolated and not determined. The slopes for both experimental and calculated curves change in the proximity of 1.5 GPa, and is likely related to a change from olivine to clinopyroxene as the liquidus phase. No experiments below the solidus temperatures were obtained, although no

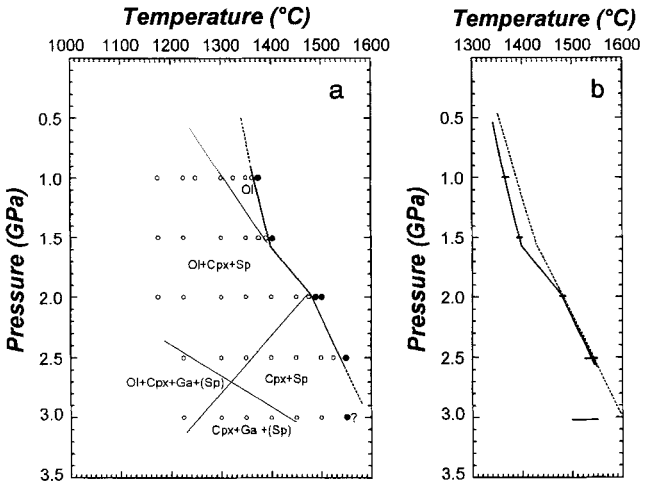

Fig 2. a. Phase relations in the P–T considered area. The heavier line represents liquidus curve. Ol = olivine, Cpx = clinopyroxene, Sp = spinel, Ga = garnet. In parentheses, phases found in very small amounts. Open circles = phases in equilibrium with melt (apart run performed at P = 3.0 GPa and T = 1225°C); solid circles = only glass present. **b.** Comparison between experimental and calculated liquidus curves. Bars represent the ranges between two runs straddling the experimental liquidus curve. Theoretical liquidus curve was calculated using MELTS software package (Ghiorso *et al.* 1994, Ghiorso & Sack 1995) considering a fO_2 at FMQ buffer.

Table II. List of runs, conditions and results.

Run #	Pressure (GPa)	Temp. (°C)	duration (min)	results
15	1.0	1300	15	Cpx, Ol, Sp, Gls
17	1.0	1250	15	Cpx, Ol, Sp, Gls
19	1.5	1350	15	Cpx, Ol, Sp, Gls, Phl, (Ilm)
21	2.0	1350	20	Cpx, Ol, Sp, Phl, Gls
22	2.5	1350	30	Cpx, Ol, Sp, Phl, Gls, (Ilm)
24	1.5	1400	20	Gls
26	1.0	1375	10	Gls
28	2.0	1400	20	Cpx, Sp, Phl, Gls, (Ol)
29	1.5	1300	40	Cpx, Ol, Sp, Gls, (Phl)
30	2.5	1400	15	Cpx, Sp, Phl, Gls
31	2.5	1450	10	Cpx, Gls, (Sp)
32	2.0	1450	10	Cpx, Ol, Phl, Sp, Gls
33	2.5	1300	25	Cpx, Sp, Phl, Gls, (Ol)
34	1.5	1225	120	Cpx, Ol, Sp, Gls, (Ilm)
35	2.0	1225	120	Cpx, Ol, Sp, Phl, Gls
36	2.5	1225	120	Cpx, Ol, Ga, Sp, Phl, Gls, (Ilm)
38	3.0	1225	150	Cpx, Ol, Ga, Sp, (Ilm)
39	3.0	1450	15	Cpx, Sp, Phl, Gls
40	3.0	1400	20	Cpx, Ga, Sp, Gls, (Phl)
41	3.0	1350	25	Cpx, Ga, Phl, Sp, Gls, (Ol)
43	3.0	1300	30	Cpx, Ga, Phl, Sp, Gls
44	1.5	1375	10	Cpx, Ol, Sp, Gls
45	2.0	1500	10	Gls
46	2.5	1500	10	Cpx, Phl, Gls
47	3.0	1500	15	Cpx, Phl, Gls
49	2.0	1475	10	Cpx, Ol, Sp, Phl, Gls
50	2.5	1550	10	Gls
53	3.0	1550	6	Gls
54	2.0	1300	30	Cpx, Ol, Sp, Phl, Gls, (Ilm)
55	1.0	1225	80	Cpx, Ol, Sp, Gls
56	1.0	1175	60	Cpx, Ol, Sp, Gls
58	1.0	1375/1350	6+1+10	Cpx, Ol, Sp, Gls
59	1.5	1175	150	Cpx, Ol, Gls
60	1.5	1375	40	Cpx, Ol, Sp, Gls, (Phl)
61	2.5	1525	10	Cpx, Phl, Gls
63	1.5	1390	10	Cpx, Ol, Sp, Gls
64	1.5	1400/1375	6+1+6	Gls
66	1.0	1325	20	Ol, Gls
67	1.0	1350	15	Cpx, Ol, Gls, (Sp)
68	1.5	1400/1350	6+3+6	Cpx, Ol, Sp, Gls
69	2.0	1175	165	Cpx, Ol, Sp, Phl, Gls, (Ilm)
70	1.5	1390	60	Ol, Gls
71	2.0	1487	10	Gls
72	2.0	1475	45	Cpx, Gls
73	1.0	1362	15	Ol, Gls, (Sp)
75	2.5	1525	40	Cpx, Phl, Gls
Runs with added H_2O: in parenthesis the amount added (in wt%):				
107 (5)	2.0	1300	30	Cpx, Ol, Sp, Phlog, Gls, (Ilm)
108 (10)	2.0	1300	30	Cpx, Ol, Sp, Phlog, Gls, (Ilm)

Ol = olivine; Cpx = clinopyroxene; Sp = spinel; Ga = garnet; Phl = phlogopite (quenching); Phlog= phlogopite (primary); Ilm = ilmenite; Gls = glass. In parentheses phases present in very small amounts. Runs #58, 64, 68 are reversal experiments (see text): the second value in the duration colon refers to the time taken to lower the temperature.

https://doi.org/10.1017/S0954102000000134 Published online by Cambridge University Press

glass was observed at 3.0 GPa, 1225°C.

One major problem with experimental runs is to evaluate the attainment of equilibrium, especially with the very short duration necessary to avoid Fe loss to the Pt capsule walls. We used various criteria to check the attainment of equilibrium:

a) Reversal experiments (e.g. Edgar 1973). Considering a near-liquidus point, duplicate runs were made reaching the run conditions from lower and higher temperatures. If the same products with similar compositions are obtained, we argue that equilibrium was achieved and the reaction is said to be reversible. This approach, however, is hindered by the silicate liquid tendency to undercool. With this in mind, three reversal experiments were carried out on points lying very close to the liquidus curve at 1.0 GPa and 1.5 GPa.

The first reversal (experiment #58) was performed at 1.0 GPa with the temperature initially at 1375°C and then dropped to 1350°C. This experiment shows the same phase assemblage (olivine + glass) as the normal experiment at 1350°C (experiment #67). Moreover, the phases show the same proportion and composition.

Two more reversals were performed at 1.5 GPa: experiment #64 (T dropped from 1400 to 1375°C) and experiment #68 (T dropped from 1400 to 1350°C). These can be compared to the normal experiments performed at the same final P–T conditions: experiments #44 (1375°C) and #19 (1350°C) respectively. In experiment #64 undercooling caused only glass to be observed unlike experiment #44 in which cpx, ol, sp and glass were detected. However, the experimental products in experiments #19 and #68 are similar, although some compositional differences still persist. In fact, phase compositions and proportions of experiment #68 are actually the same as those found in experiment #44 at higher T (1375°C). These discrepancies are probably caused by undercooling (ΔT) effects. The obtained ΔT's (15–50°C at P = 1.5 GPa and 25°C at P = 1.0 GPa) are consistent with the values obtained considering similar compositional systems (e.g. Donaldson 1979).

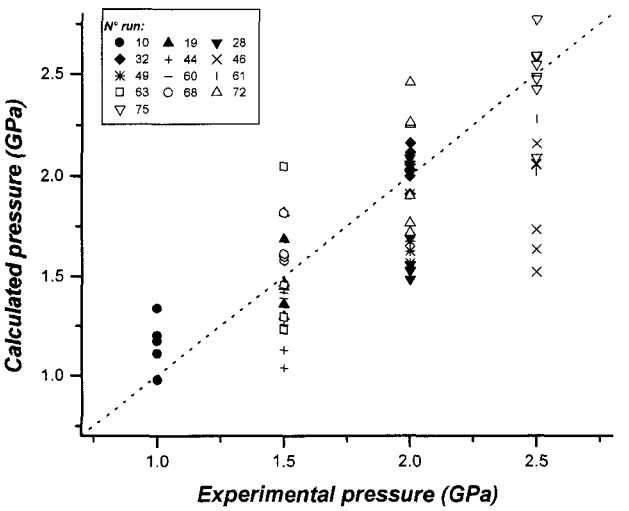

Fig. 3. Representation of the application of Nimis (1995) geobarometer on rim clinopyroxenes crystallized in near liquidus conditions ($T_{liq.}$–$T_{crist.}$<50°C) up to 2.5 GPa, in absence of garnet.

b) Experiments of variable duration under the same P and T conditions. Several run pairs with variable duration were performed (i.e., experiments #44–60, #63–70, #49–72, #61–75). In general, at near-liquidus conditions, short duration runs (about 10 min) yield unclear results because of the presence of too many phases. Long duration (40–60 min) experiments unequivocally show liquidus phase even if Fe losses could have considerably changed the chemical composition of the system.

c) Geothermobarometers. Several geothermobarometers have been applied to run products to check attainment of equilibrium. The Nimis (1995) geobarometer was applied to clinopyroxene rims crystallized in absence of garnet under near-liquidus conditions ($T_{liq.}$–$T_{crist.}$<50°C) up to 2.5 GPa. Although there is a good agreement between mean calculated values and experimental pressures (Fig. 3), some scattering is evident. This can be due either to the uncertainty of the geobarometer (± 0.2 GPa) or to incomplete attainment of equilibrium in some crystal rims. The major scattering at 2.5 GPa is probably due also to the fact that this pressure exceeds the upper limit of the geobarometer calibration (i.e. 2.4 GPa, Nimis 1995).

The clinopyroxene-garnet geothermometer using the calibrations of Råheim & Green (1974), Ellis & Green (1979) and Pattison & Newton (1989) gives the best values (± 100°C) if crystal rim compositions are used. The poorest results were obtained with the Pattison & Newton (1989) calibration, owing probably to the upper limit (1200°C) in which it was calibrated. This temperature is lower than all run temperatures in which garnet was found. The upper calibration limits used by Råheim & Green (1974), and Ellis & Green (1979) are 1400°C and 1300°C, respectively.

Another criterion for evaluating attainment of equilibrium is given by the Fe/Mg exchange between olivine and melt. Considering the runs where olivine coexists only with melt, the K_d(Fe/Mg) between the two phases is in the range between 0.27 and 0.33, compared to the equilibrium value of 0.30 (Roeder & Emslie 1970, Gerlach & Grove 1982).

Although complete equilibrium was not completely achieved in short duration runs, it was strongly suggested that at the crystal scale, rims equilibrated with glasses. This is further demonstrated by the similarity of products of reversal experiments and by the close agreement between calculated and observed liquidus curves.

https://doi.org/10.1017/S0954102000000134 Published online by Cambridge University Press

Mineral composition

Olivine usually has subeuhedral shape with a Fo content ranging from 65 to 94 mol% (Table III). Sometimes it shows a "skeletal" habit (Fig. 4) suggesting of high cooling rate and/or the undercooling of the melt. Generally, rims of near-liquidus olivines have a greater Fo content respect to the rims of lower T crystals. MnO and CaO contents are not strictly dependent on either P and T and they vary up to 0.9 and 1.5 wt% respectively. In some near liquidus runs performed at 1.0 and 1.5 GPa, melt inclusions are found in olivine (Fig. 5); mass balance calculations indicate olivine crystallization variable from 11 to 17 wt% after the trapping of melt inclusions.

Garnet crystallizes after clinopyroxene and is a predominantly pyrope (45–70 mol%)-almandine (5–35 mol%) solid solution (Table IV). TiO_2 contents are high (up to 3 wt%) and comparable with those of garnets synthesized in melting experiments of metabasalts from 1.6 GPa to 3.6 GPa (Rapp & Watson 1995) and of H_2O saturated basalts in the range of 1.8 to 3.6 GPa (Green & Ringwood 1968). MgO contents sharply decrease (from 19 wt% to 12 wt%) in crystals grown at 3.0 GPa and 1225°C, probably due to the coexistence with olivine in this run. The grossular end-member does not increase with T as in experiments performed by Green (1977).

Clinopyroxene is usually euhedral and is represented by Ca–Mg–Fe and Na–Ca pyroxenes (Table V); diopside is prevalent at 1.0 GPa, augite predominates at higher P whilst omphacite

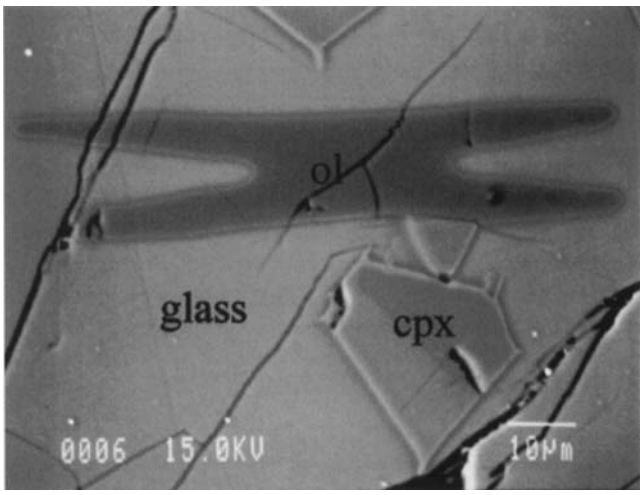

Fig. 4. Backscattered electron microphotograph showing a crystal of skeletal olivine immersed in the glass, beside an euhedral zoned clinopyroxene crystal (P = 1.5 GPa, T = 1350°C).

is detected only at P = 2.5 GPa. The Na contents increases in the M2 site with increasing P, as a consequence of the entry of trivalent cations (R^{3+}) in the M1 site (Fig. 6). Moreover, as stated by White (1964) and Herzberg & Chapman (1976) ^{VI}Al and ^{IV}Al generally increase with P and T respectively. In Fig. 7a & b these two values are plotted against P (at T = 1300°C) and T (at P = 2.5 GPa) respectively. In Fig. 7b a

Table III. Representative analyses of olivine from charges.

Run #	67	15	17	56	63	34	32	21	35	36
Spot #	67–8	15–30	17–2	56–18	63–9	34–7	32–17	21–26	35–9	36–29
P (GPa)	1	1	1	1	1.5	1.5	2	2	2	2.5
T (°C)	1350	1300	1250	1175	1390	1225	1450	1350	1225	1225
SiO_2	41.0	40.6	39.5	41.1	40.3	37.5	41.4	40.0	39.5	39.8
TiO_2	0.07	bdl	0.04	0.04	0.06	0.10	0.03	0.04	0.05	0.06
Al_2O_3	0.02	0.07	0.04	0.10	0.03	0.09	0.06	0.13	0.26	0.73
Cr_2O_3	bdl	0.09	0.03	0.06	bdl	0.04	0.17	0.03	bdl	bdl
FeO	9.92	13.0	12.2	11.7	13.5	25.0	10.4	13.2	17.9	20.6
MnO	0.24	0.26	0.21	0.15	0.11	0.39	0.24	0.22	0.25	0.24
NiO	0.17	0.26	0.24	na	na	na	na	0.22	na	0.18
MgO	49.2	46.3	47.1	46.7	47.2	37.3	48.2	46.6	42.6	39.5
CaO	0.49	0.36	0.32	0.22	0.31	0.45	0.26	0.34	0.32	0.82
Sum	101.2	100.9	99.7	100.0	101.5	100.9	100.8	100.8	100.9	101.9
Si	0.996	1.002	0.986	1.013	0.990	0.983	1.009	0.990	0.996	1.006
Ti	0.001	0.000	0.001	0.001	0.001	0.002	0.001	0.001	0.001	0.001
Al	0.001	0.002	0.001	0.003	0.001	0.003	0.002	0.004	0.008	0.022
Cr	0.000	0.002	0.001	0.001	0.000	0.001	0.003	0.001	0.000	0.000
Mg	1.782	1.701	1.752	1.716	1.729	1.457	1.749	1.720	1.603	1.486
Ni	0.003	0.005	0.005	0.000	0.000	0.000	0.000	0.004	0.000	0.004
Fe	0.201	0.268	0.254	0.241	0.277	0.547	0.213	0.274	0.377	0.436
Mn	0.005	0.005	0.004	0.003	0.002	0.009	0.005	0.005	0.005	0.005
Ca	0.013	0.010	0.009	0.006	0.008	0.013	0.007	0.009	0.009	0.022
Z	0.996	1.002	0.986	1.013	0.990	0.983	1.009	0.990	0.996	1.006
Y	2.005	1.993	2.026	1.970	2.018	2.029	1.978	2.016	2.002	1.975
Fo	89.8	86.4	87.3	87.7	86.2	72.7	89.2	86.3	80.9	77.3

bdl = below detection limit, na = not analysed, Fo = forsterite (mol%).

https://doi.org/10.1017/S0954102000000134 Published online by Cambridge University Press

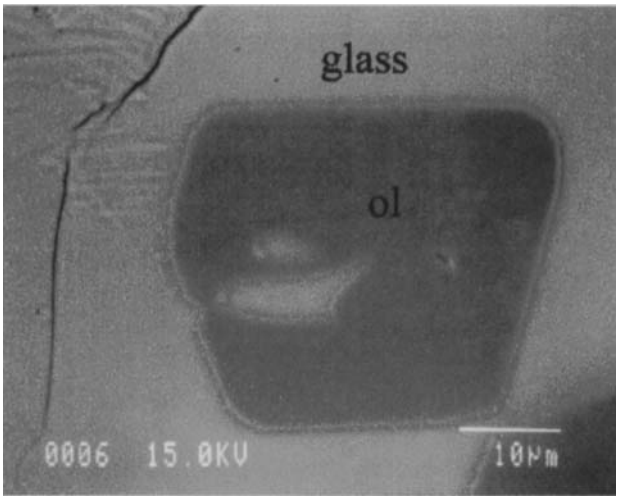

Fig. 5. Backscattered electron microphotograph showing an euhedral olivine crystal with a melt inclusion in glass. Mass balance calculations indicate that composition of the melt is from crystallization of about 11 vol% of the host, suggesting the vicinity with liquidus curve (P = 1.5 GPa, T = 1390°C).

decrease of ^{IV}Al at the higher T is matched by the absence of spinel; this phase is present in all the other charges at P = 2.5 GPa.

Spinel has the widest compositional range among all analysed mineral phases (Table VI). Compositions synthesized at T = 1350°C are reported in Fig. 8, and compared with fields of three spinel types found in lherzolitic xenoliths (Carswell 1980). All crystals synthesized at 1.0 GPa are Cr-spinels whereas all the others are Cr- and Al-spinels. Ülvospinel end-member reaches values up to 60 mol%.

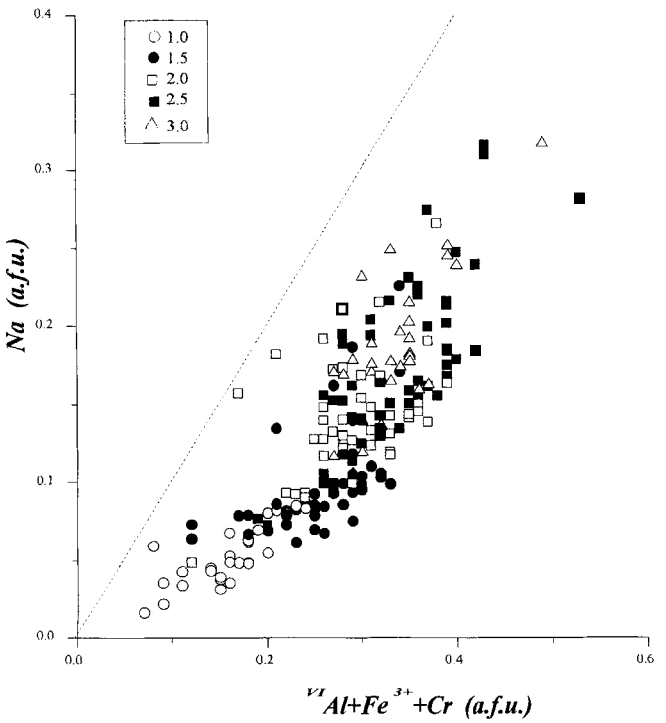

Fig. 6. Trivalent cations (R^{3+}) vs Na contents in experimental clinopyroxene rims. Crystallization pressures (in GPa) are shown in legend. The distance from the dotted line shows how much of the trivalent are charge balancing for Na.

Table IV. Representative analyses of garnet from charges.

Run #	36	40	43	38
Spot #	36–26	40–8	43–16	38–22
P (GPa)	2.5	3	3	3
T (°C)	1225	1400	1300	1225
SiO_2	41.8	40.0	41.0	39.3
TiO_2	1.94	2.80	1.23	1.94
Al_2O_3	20.7	20.9	20.9	21.0
Cr_2O_3	0.07	0.17	0.17	0.09
FeO	13.9	12.1	13.0	16.1
MnO	0.42	0.30	0.34	0.45
MgO	14.9	17.4	17.1	13.6
CaO	7.79	6.97	6.60	8.22
Na_2O	0.33	0.18	0.35	0.28
Sum	101.8	100.8	100.6	101.0
Oxides recalculated on the basis of the mineral formula:				
FeO	13.0	8.96	9.18	12.1
Fe_2O_3	0.94	3.50	4.23	4.43
# of cations on the basis of 24 oxygens:				
Si	6.025	5.758	5.902	5.760
Al^{IV}	0.000	0.242	0.098	0.240
Al^{VI}	3.515	3.312	3.454	3.395
Cr	0.008	0.019	0.019	0.010
Ti	0.211	0.303	0.133	0.214
Fe^{3+}	0.102	0.380	0.459	0.490
Mg	3.211	3.729	3.669	2.973
Fe^{2+}	1.577	1.080	1.103	1.486
Mn	0.051	0.037	0.042	0.056
Ca	1.204	1.076	1.019	1.292
Na	0.092	0.050	0.098	0.080
X	6.139	5.972	5.933	5.890
Y	3.836	4.015	4.067	4.110
Z	6.025	6.000	6.000	6.000
Uv	0.2	0.5	0.5	0.3
Ad	2.8	9.9	11.8	12.7
Py	59.0	64.7	62.9	51.6
Sp	0.9	0.6	0.7	1.0
Gr	19.1	8.3	5.2	9.4
Al	17.9	16.0	18.9	25.0
Mg#	67.1	77.5	76.9	66.7

End-members (in mol%) calculated according to Rickwood (1968): Uv = uvarovite, Ad = andradite, Py = pyrope, Sp = spessartine, Gr = grossular, Al = almandine. Mg# = 100*Mg/(Mg + Fe^{2+}).

Mica is only found in glasses and it always has a lathlike shape (Fig. 9a). Compositionally, it ranges from phlogopite to Fe-biotite. The lathlike shape of the mica suggests that it is a quenched phase. The quenched nature of the mica is also suggested by the high and variable TiO_2 content ranging from 4 to 11 wt% (Yoder & Kushiro 1969, Edgar *et al.* 1976, Lloyd *et al.* 1985) even if, according to Forbes & Flower (1974), such Ti-rich micas can be stable at 3.0 GPa, up to 1500°C in

https://doi.org/10.1017/S0954102000000134 Published online by Cambridge University Press

Table V. Representative analyses of clinopyroxene from charges.

Run #	15	55	44	34	72	35	61	36	39	38
Spot #	15–22	55–32	44–26	34–23	72–14	35–6	61–20	36–33	39–2	38–3
P (GPa)	1	1	1.5	1.5	2	2	2.5	2.5	3	3
T (°C)	1300	1225	1375	1225	1475	1225	1525	1225	1450	1225
SiO_2	48.1	48.9	47.4	48.0	44.7	48.3	47.7	48.3	49.6	50.1
TiO_2	1.96	1.95	1.54	2.52	5.07	2.38	1.32	1.94	1.30	1.64
Al_2O_3	8.21	9.50	10.0	10.5	17.7	11.5	11.9	11.8	10.7	9.26
Cr_2O_3	0.45	0.21	0.22	0.07	0.04	0.04	0.14	0.11	0.08	0.12
FeO	4.82	5.86	6.19	9.16	2.87	7.62	6.40	8.74	7.41	8.23
MnO	0.22	0.15	0.13	0.17	0.20	0.18	0.15	0.19	0.23	0.14
MgO	14.5	13.7	13.9	12.5	13.3	12.8	14.6	12.7	15.7	12.4
CaO	20.7	19.4	18.7	15.2	12.6	14.1	15.6	13.3	12.4	13.8
Na_2O	0.68	0.98	1.10	2.29	2.71	2.42	1.93	2.50	2.76	3.50
Sum	99.7	100.6	99.2	100.3	99.2	99.3	99.8	99.7	100.2	99.1
Oxides recalculated on the basis of the mineral formula:										
FeO	3.49	5.86	3.97	7.16	2.87	7.54	3.13	8.00	3.56	5.23
Fe_2O_3	1.48	–	2.47	2.23	–	0.09	3.63	0.82	4.28	3.34
# of cations on the basis of 24 oxygens:										
Si	1.765	1.780	1.742	1.754	1.616	1.770	1.727	1.767	1.776	1.832
Al^{IV}	0.235	0.220	0.258	0.246	0.384	0.230	0.273	0.233	0.224	0.168
Fe^{3+}	0.000	0.000	0.000	0.000	0.000	0.000	0.000	0.000	0.000	0.000
Sum T	2.000	2.000	2.000	2.000	2.000	2.000	2.000	2.000	2.000	2.000
Al^{VI}	0.121	0.188	0.176	0.206	0.371	0.267	0.233	0.277	0.228	0.231
Fe^{3+}	0.041	0.000	0.068	0.061	0.000	0.002	0.099	0.023	0.115	0.092
Ti	0.054	0.053	0.043	0.069	0.138	0.066	0.036	0.053	0.035	0.045
Mg	0.771	0.744	0.707	0.661	0.490	0.664	0.628	0.643	0.619	0.629
Cr	0.013	0.006	0.006	0.002	0.001	0.001	0.004	0.003	0.002	0.003
Fe^{2+}	0.000	0.009	0.000	0.000	0.000	0.000	0.000	0.000	0.000	0.000
Sum M1	1.000	1.000	1.000	1.000	1.000	1.000	1.000	1.000	1.000	1.000
Na	0.048	0.069	0.078	0.162	0.190	0.172	0.135	0.177	0.192	0.248
Mn	0.007	0.005	0.004	0.005	0.006	0.006	0.005	0.006	0.007	0.004
Ca	0.816	0.756	0.738	0.593	0.487	0.555	0.606	0.521	0.477	0.542
Fe^{2+}	0.107	0.170	0.122	0.219	0.087	0.231	0.095	0.245	0.107	0.160
Mg	0.022	0.000	0.057	0.020	0.230	0.036	0.159	0.051	0.217	0.046
Sum M2	1.000	1.000	1.000	1.000	1.000	1.000	1.000	1.000	1.000	1.000
M1+M2	2.000	2.000	2.000	2.000	2.000	2.000	2.000	2.000	2.000	2.000
O	6.000	6.006	6.000	6.000	6.037	6.000	6.000	6.000	6.000	6.000
Q	1.7	1.7	1.6	1.5	1.3	1.5	1.5	1.5	1.4	1.4
J	0.1	0.1	0.2	0.3	0.4	0.3	0.3	0.4	0.4	0.5
Wo	46.2	44.9	43.5	38.0	37.5	37.2	38.1	35.0	30.9	36.8
En	45.0	44.2	45.0	43.7	55.4	46.8	49.4	46.7	54.2	45.8
Fs	8.8	10.9	11.5	18.3	7.2	16.0	12.5	18.4	14.9	17.4
Mg #	88.1	80.6	86.2	75.7	89.2	75.1	89.2	73.9	88.7	80.8

cations calculated according to Morimoto *et al.* (1988). Wo = wollastonite (mol%), En = enstatite (mol%), Fs = ferrosilite (mol%).

vapour-free systems. Moreover, the quenched origin is supported by the Mg# (= $Mg/(Mg+Fe^{2+})$), which does not increase with T (at the same P) as generally observed for the other phases. Although mica is not a primary phase in the investigated conditions, its presence as a quenched phase suggests that the conditions are not far from those under which mica is stable. It is possible that an increase in the activity of H_2O could stabilize mica as a primary phase. To check this possibility, two experiments with 5 and 10 wt% of H_2O added, respectively, were performed at 2.0 GPa and 1300°C. These P–T conditions are not too close to the liquidus (the addition of water can bring a point near the liquidus in "*supra-liquidus*" conditions) but not too far either, so that the kinetic efficiency is not too low. In both experiments, the phases detected were the same as in the experiment performed without any H_2O added. Nevertheless, in the experiments performed with added H_2O, the mica attains a prismatic habit with size ranging from 10 to 30 μm, strongly suggesting its stability as a primary phase. Mica, synthesized in experiments performed without adding water and in hydrated conditions are shown in Fig. 9a & b respectively, and their chemical compositions are reported in Table VII. Apparently, no significant differences were noticed between the two H_2O-added experimental products. Note the high TiO_2 contents of primary mica compared to the

https://doi.org/10.1017/S0954102000000134 Published online by Cambridge University Press

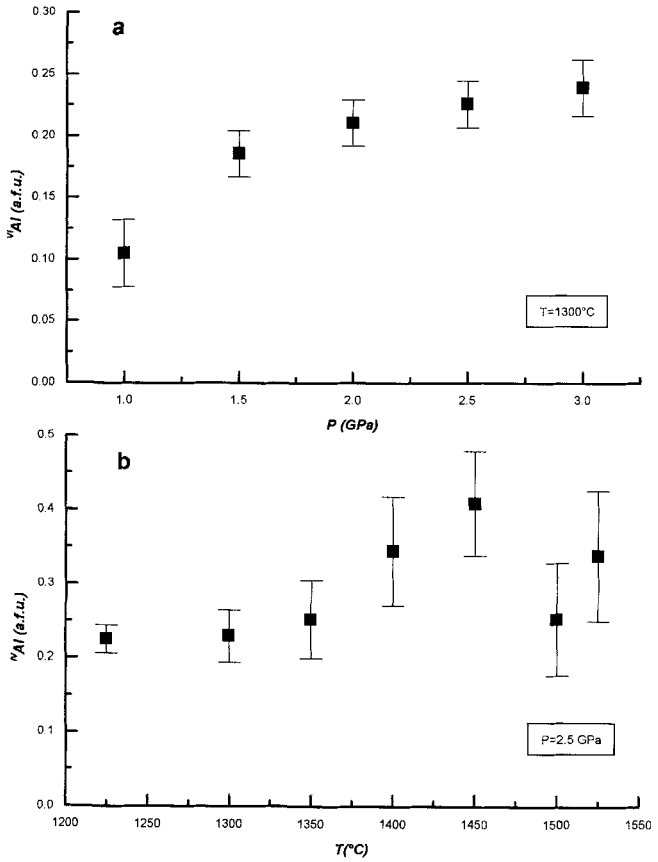

Fig. 7. a. ^{VI}Al vs P in clinopyroxene rims, **b.** ^{IV}Al vs T in clinopyroxene rims. Bar represents standard deviation calculated on the base of the compositional range for each run.

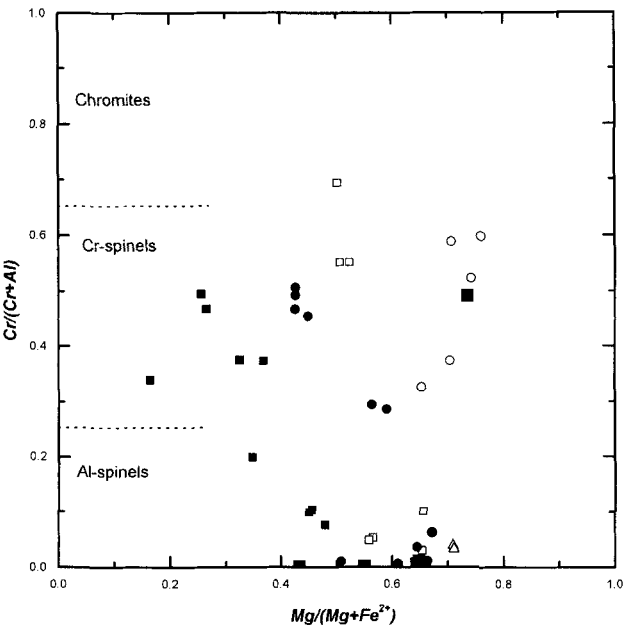

Fig. 8. Mg/(Mg+Fe^{2+}) vs Cr/(Cr+Al) in spinels for experiments performed at T = 1350°C. Symbols as in Fig. 6.

values relative to mica synthesized in experiments performed without adding water; hence, even if some authors state that Ti-rich micas are likely to represent a quenched phase (see above), at least in the present case, this is not true. This difference in TiO_2 abundance between primary and quenched crystals can be due to the highly refractory nature of the primary mica (stable at the P–T conditions of the run) relative to the non-primary one (stable at lower T). On the other hand, the Na_2O and CaO contents seems to better discriminate between primary and quenched crystals; the primary crystals have Na_2O < 0.65 wt% and CaO < 0.30 wt%, whereas the quenched crystals have Na_2O in the range 1.0–4.9 wt% and CaO in the range 0.4–7.0 wt% (Table VII).

Inferences on the origin of magma

Orthopyroxene was not found in any run. This absence is common in many experimental studies on basalts (e.g. Allen

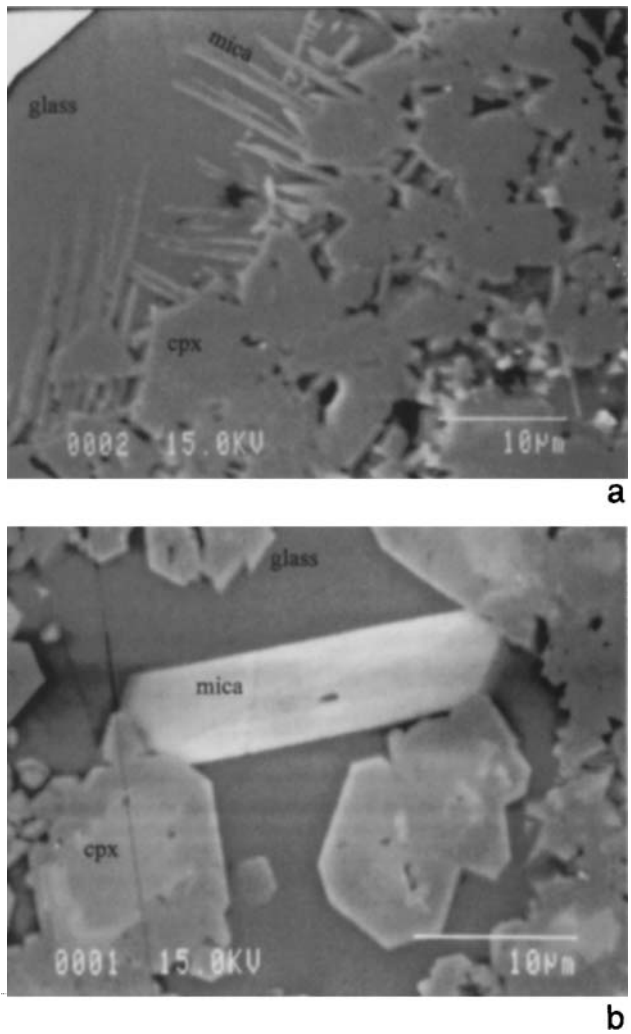

Fig. 9. a. Microphotograph of quenched mica grown in the glass around clinopyroxene (P = 2.0 GPa, T = 1300°C, H_2O = 0.65 wt%), **b.** Microphotograph of primary mica (P = 2.0 GPa, T = 1300°C, H_2O = 5.65 wt%).

https://doi.org/10.1017/S0954102000000134 Published online by Cambridge University Press

Table VI. Representative analyses of spinel from charges.

Run #	67	15	44	68	49	54	30	33	39	43
Spot #	67–4	15–35	44–11	68–27	49–7	54–15	30–7	33–7	39–9	43–39
P (GPa)	1	1	1.5	1.5	2	2	2.5	2.5	3	3
T (°C)	1350	1300	1375	1350	1475	1300	1400	1300	1450	1300
SiO_2	0.19	0.71	0.09	0.25	0.37	0.62	1.04	0.11	4.63	0.14
TiO_2	1.27	3.28	0.87	2.99	0.98	2.60	1.12	2.57	1.25	0.96
Al_2O_3	22.3	20.8	24.2	43.5	55.6	45.3	55.0	28.7	50.8	20.1
Cr_2O_3	36.4	34.0	38.6	bdl	0.19	3.41	0.25	24.4	0.75	41.2
FeO	20.2	27.2	19.0	38.0	23.5	32.2	22.2	29.2	22.1	24.1
MnO	bdl	bdl	bdl	0.19	0.21	0.10	0.13	0.09	0.16	bdl
MgO	16.9	12.8	15.9	14.0	19.0	15.4	19.7	13.2	19.3	12.1
CaO	0.32	0.50	0.14	0.15	0.13	0.25	0.26	0.34	1.46	0.52
Na_2O	bdl	na	0.05	bdl	0.05	0.12	na	na	na	na
K_2O	0.03	na	bdl	0.02	0.03	0.05	na	na	na	na
NiO	na	0.13	na	na	na	na	bdl	0.18	0.31	0.14
ZnO	na	0.13	na	na	na	na	0.02	0.12	0.10	0.15
Sum	97.5	99.6	98.9	99.1	100.0	100.0	99.7	99.0	100.8	99.4
Oxides recalculated on the basis of the mineral formula:										
Fe_2O_3	10.84	8.67	7.63	19.64	11.56	14.89	10.48	12.10	5.36	7.40
FeO	10.42	19.39	12.16	20.36	13.11	18.80	12.82	18.36	17.25	17.43
Formula on the basis of 24 cations:										
Fe^{2+}	2.131	4.038	2.456	3.836	2.291	3.475	2.240	3.709	3.055	3.670
Mn	0.000	0.000	0.000	0.036	0.037	0.019	0.023	0.018	0.029	0.000
Mg	6.148	4.752	5.723	4.690	5.903	5.075	6.129	4.765	6.095	4.547
Sum A	8.279	8.790	8.179	8.562	8.231	8.568	8.393	8.493	9.179	8.217
Si	0.046	0.177	0.022	0.056	0.077	0.137	0.217	0.027	0.980	0.035
Ti	0.233	0.614	0.158	0.506	0.154	0.432	0.176	0.467	0.199	0.182
Al	6.421	6.109	6.883	11.545	13.689	11.791	13.526	8.154	12.662	5.971
Cr	7.025	6.686	7.371	0.000	0.031	0.595	0.041	4.661	0.126	8.194
Fe^{3+}	1.995	1.624	1.386	3.330	1.818	2.477	1.647	2.200	0.854	1.401
Sum B	15.720	15.210	15.820	15.438	15.769	15.432	15.607	15.507	14.821	15.783
Mg#	74.3	54.1	70.0	55.0	72.0	59.3	73.2	56.2	66.6	55.3

bdl = below detection limit; na = not analysed. Mg# = $100*Mg/(Mg+Fe^{2+})$.

et al. 1975, Arculus 1975, Maaløe & Jakobsson 1980) and may be explained by a reaction relationship between orthopyroxene and the liquid at the source. Experimental studies on peridotitic compositions within the CMAS system have demonstrated that enstatite is in reaction relationship with the liquid generated in the first stage of partial melting (Maaløe & Petersen 1976, Wyllie & Huang 1976). In our starting material, this can be deduced by the rare orthopyroxene found as xenocrysts in the natural sample. In this case, orthopyroxene could come from mantle xenoliths, representing the source of the investigated basanite. Another explanation can be provided by the paucity of CO_2 in the starting material; this component indeed tends to stabilize orthopyroxene with respect to olivine and clinopyroxene (Eggler 1974, 1978). If we accept this, we must assume that the investigated basanite lost some CO_2 during its ascent to the surface. Finally, some authors (e.g. Green *et al.* 1979, Stolper 1980) suggest that orthopyroxene is never on the liquidus if starting materials with MgO < 13 wt% are considered. This is compatible with the results of this petrological investigation (MgO in the studied basanite is 12.5 wt%).

Assuming that the absence of orthopyroxene can be justified, multiple saturation with a lherzolitic source can occur when olivine, clinopyroxene and an Al-phase (plagioclase, spinel or garnet) are stable at near-liquidus conditions. This seems to be verified when the liquidus phase change occurs, that is at 1.5–2.0 GPa and 1390–1490°C. It is therefore possible that liquid was generated in these P–T conditions by a spinel lherzolite mantle source. Nevertheless if the garnet in line in Fig. 2a is extended, it probably intersects the extended liquidus curve at 3.2–3.5 GPa at T > 1550°C. It is likely that above this pressure garnet becomes a liquidus phase. Thus, the primary liquid could also have been generated from a garnet pyroxenite source at pressures above 3.2 GPa. A garnet lherzolite mantle source, however, can be ruled out because olivine and garnet never coexist near the liquidus.

In summary, on the basis of our experimental results, two hypotheses can be formulated about the nature of the mantle source and the P–T conditions in which the basanite liquid was generated:

i) spinel lherzolite (at 1.5–2.0 GPa and 1390–1490°C),

ii) garnet pyroxenite (at 3.2–3.5 GPa at > 1550°C).

Both hypotheses have to be evaluated in the context of other

https://doi.org/10.1017/S0954102000000134 Published online by Cambridge University Press

Table VII. Representative analyses of mica from charges performed at P = 2.0 GPa and T = 1300°C.

Run #	54	54	107	107	108	108
Spot #	17	25	1	5	2	4
H_2O (wt%) added	0	0	5	5	10	10
q/p	q	q	p	p	p	p
SiO_2	38.1	39.1	36.1	35.7	35.6	35.7
TiO_2	8.34	8.36	12.4	12.9	11.9	11.5
Al_2O_3	15.2	15.7	15.3	14.8	15.2	15.8
Cr_2O_3	0.02	0.06	bdl	bdl	0.05	0.07
FeO	15.0	15.3	9.49	12.2	12.5	12.0
MnO	0.09	0.11	0.11	0.05	0.03	0.03
MgO	9.90	8.00	12.7	11.3	12.1	12.2
CaO	0.82	1.30	0.21	0.14	0.22	0.26
Na_2O	2.00	1.80	0.46	0.60	0.50	0.62
K_2O	7.47	7.23	8.39	8.25	8.55	8.54
SrO	na	na	0.21	0.27	0.23	0.25
BaO	na	na	1.63	1.68	2.25	1.90
F	na	na	0.96	0.64	0.68	1.09
SO_3	na	na	0.06	0.14	0.10	0.09
Cl	na	na	0.02	bdl	0.04	0.03
O = F, Cl			0.40	0.27	0.28	0.45
Sum	97.0	97.0	97.8	98.4	99.8	100.2
Numbers of ions on the basis of 22 oxygens:						
Si	5.565	5.694	5.258	5.237	5.187	5.183
Al^{IV}	2.435	2.306	2.624	2.554	2.619	2.711
Ti^{IV}	0.000	0.000	0.118	0.209	0.194	0.106
Al^{VI}	0.183	0.384	0.000	0.000	0.000	0.000
Ti^{VI}	0.916	0.915	1.237	1.218	1.117	1.152
Fe^{2+}	1.833	1.862	1.156	1.495	1.524	1.462
Mn	0.011	0.014	0.014	0.006	0.004	0.004
Mg	2.156	1.735	2.791	2.461	2.640	2.655
Cr	0.002	0.007	0.000	0.000	0.006	0.008
Ca	0.128	0.203	0.033	0.022	0.034	0.040
Na	0.566	0.508	0.130	0.170	0.141	0.175
K	1.392	1.342	1.558	1.543	1.591	1.583
Z	8.000	8.000	8.000	8.000	8.000	8.000
Y	5.102	4.916	5.198	5.181	5.290	5.280
X	2.086	2.052	1.721	1.735	1.766	1.799
Sum	15.188	14.968	14.919	14.916	15.056	15.079
Mg #	54.0	48.2	70.7	62.2	63.4	64.5

q = quenching crystal, p = primary crystal, bdl = below detection limit, na = not analysed

studies on the primitive volcanic rocks of this volcanic region, to evaluate which one would be more compatible with the petrology of this suite of rocks. In this respect, the following points are of interest:

a) Orlando *et al.* (1997) have shown that the onset of crystallization of the rocks considered here occurs between 1250°C and 1300°C at 2.0 to 2.5 GPa. These results would exclude the spinel lherzolite source hypothesis because crystallization would occur deeper than depth of generation.

b) Considering the rare-earth pattern normalised to chondrite, Armienti *et al.* (1991, 1997) established that garnet is a likely residual phase in the mantle during partial melting. This conclusion seems also to exclude the first hypothesis. However, this statement is valid if we do not consider the possibility of a metasomatized source. The rapid ascent of the basanite liquid to the surface (this should be true if we assume that the basanite has a near "primary" composition) would exclude the hypothesis that the liquid could have re-equilibrated in spinel field.

c) The geotherm calculated on the basis of geothermobarometry of granulitic xenoliths enclosed in MMVG lavas (Berg *et al.* 1989) indicates that at 1.5 GPa, the temperature is around 900–1000°C. Extrapolating this geotherm up to 2.0 GPa, a maximum temperature of 1100°C is obtained. It is, therefore, difficult to accept that the primary liquid was generated under conditions compatible with a spinel lherzolite source. These conditions would imply indeed a very high geothermal gradient, greater than the average geothermal gradient in mid-ocean ridge areas.

All these considerations seem to favour the garnet pyroxenite source hypothesis. Furthermore, it has been proved that the addition of at least 5 wt% of H_2O stabilizes the mica; therefore this mineral can be a residual phase during mantle partial melting if it is assumed that some water was lost during the ascent of the liquid.

Phlogopite pyroxenites are thought to be a possible source of alkali-rich magmas (e.g. Wass 1980, Wass & Rogers 1980). The presence of mica, together with the experimental evidence of the possible pyroxenite source, would constitute an indication of a metasomatized mantle source. Subcrustal mica- and amphibole-bearing xenoliths enclosed in lavas of MMVG are a further evidence of a metasomatized mantle source. The presence of hydrous phases in the mantle beneath the area is also shown by the mineralogy of mantle xenoliths enclosed in the most primitive of MMVG volcanic rocks (e.g. Gamble *et al.* 1988, Beccaluva *et al.* 1991b, Hornig *et al.* 1991).

If the garnet pyroxenite hypothesis is accepted, the "low" temperatures of the beginning of crystallization (1250–1300°C; Orlando *et al.* 1997) have to be explained. The shape of the liquidus curve (Fig. 2) suggests that adiabatic decompression of the primary liquid caused an overheating of the liquid itself, allowing achievement of the calculated temperatures of onset of crystallization without changing its composition. Furthermore, the presence in the source of higher amounts of H_2O than that of starting material (LOI–CO_2 = 0.85–0.20 = 0.65 wt%, see Table I) can lower the generation temperature of the primary liquid and cause it to approach its liquidus temperature. The presence of higher amounts of H_2O in the source is also consistent with mica being a residual phase during mantle partial melting.

Conclusions

Based upon our experimental results, two hypotheses can be

https://doi.org/10.1017/S0954102000000134 Published online by Cambridge University Press

formulated for the source of near "primary" magma: a spinel lherzolite or a garnet pyroxenite. In the former case segregation would have occurred at 1.5–2.0 GPa at GPa and 1390–1490°C, in the latter at > 3.0 GPa (presumably at 3.2–3.5 GPa) at > 1550°C. A comparison with the results obtained in a previous paper evaluating phase equilibria among primitive rocks suggests a garnet pyroxenite source. Furthermore, mica can represent a residual phase in the source if it is assumed that the liquid lost some H_2O during its ascent. A phlogopite-bearing garnet pyroxenite source suggests the occurrence of mantle metasomatism prior to partial melting.

In Victoria Land, a region with positive heat anomaly associated with magmatism, melt generation and segregation seem to be controlled by local extension provided by a wider-scale regional transtensional domain. Experimental data discussed in this paper show that a major role in the generation of primitive basanitic magma is played by a metasomatized mantle source. In this context the evaluation of the role played by an active mantle plume in melt generation needs to be carefully investigated extending experimental work to less alkaline magmas that are abundant in the region.

Acknowledgements

The authors wish to thanks Y. Thibault, A.D. Edgart, P. Kyle, J. Gamble and P. Manetti for the helpful discussions, support and criticism on an early draft of the manuscript; P. Ulmer for suggestions in calibrating the piston cylinder; F. Olmi and G. Vaggelli for skilful assistance during microprobe analyses; L. Francalanci for performing INAA analyses; O. Vaselli and L. Giannini for helping with wet chemical analyses. S.C. wish to thank G. Brey, Y. Thibault, S.F. Foley, F. Barbetti, R. Weber, R. Shirran who helped with the experimental laboratory at the University of Florence.

Financial support was provided by the "Progetto Nazionale Ricerche in Antartide" (P.N.R.A.) and by C.N.R. by means grants #97.00407, 95.04064 & 96.01818. The senior author (A.O.) benefited of a M.U.R.S.T. doctoral fellowship.

References

Allen, J.C., Boettcher, A.L. & Marland, G. 1975. Amphiboles in andesite and basalt: I. Stability as a function of P–T-fO_2. *American Mineralogist*, **60**, 1069–1085.

Arculus, R.J. 1975. Melting behavior of two basanites in the range 10–35 kbar and the effect of TiO_2 on the olivine-diopside reactions at high pressures. *Yearbook Carnegie Institution of Washington*, **74**, 512–515.

Armienti, P., Francalanci, L. & Salvioli, E. 1994. Petrogenesis of the McMurdo Volcanic Group and its bearing on the recent evolution of the crust-mantle system in Northern Victoria Land. *Terra Antartica*, **1**, 533–535.

Armienti, P., Francalanci, L., Landi, P. & Vita, G. 1997. Age and geochemistry of volcanic rocks from Daniell Peninsula and Coulman Island, Hallett volcanic province, Antarctica. *Geologische Jahrbuck*, in press.

Armienti, P., Tonarini, S., Innocenti, F. & Francalanci, L. 1995. Cenozoic magmatism between Priestly and Tucker glaciers, Northern Victoria Land, Antarctica. *In* Ricci, C.A., *ed. The Antarctic region: geological evolution and processes*. Siena: Terra Antartica Publication, 13.

Armienti, P., Civetta, L., Innocenti, F., Manetti, P., Tripodo, A., Villari, L. & Vita, G. 1991. New petrological and geochemical data on Mt. Melbourne volcanic field, Northern Victoria Land, Antarctica. (II Italian Antarctic expedition). *Memorie della Società Geologica Italiana*, **46**, 397–424.

Beccaluva, L., Civetta, L., Coltorti, M., Orsi, G., Saccani, E. & Siena, F. 1991a. Basanite to tephrite lavas from Melbourne volcanic province, Victoria Land, Antarctica. *Memorie della Società Geologica Italiana*, **46**, 383–395.

Beccaluva, L., Coltorti, M., Orsi, G., Saccani, E. & Siena, F. 1991b. Nature and evolution of the sub-continental lithospheric mantle of Antarctica: evidence from ultramafic xenoliths of the Melbourne volcanic province (Northern Victoria Land, Antarctica). *Memorie della Società Geologica Italiana*, **46**, 353–370.

Bence, A.E. & Albee, A.L. 1968. Empirical correction factors for the electron microanalysis of silicates and oxides. *Journal of Geology*, **76**, 382–402.

Berg, J.H., Moscati, R.J. & Herz, D.L. 1989. A petrologic geotherm from a continental rift in Antarctica. *Earth and Planetary Science Letters*, **93**, 98–108.

Biggar, G.M. 1977. Some disadvantages of $Pt_{95}Au_5$ as a container for molten silicates. *Mineralogical Magazine*, **41**, 555–556.

Bohlen, S.R.B., Essene, E.J. & Boettcher, A.L. 1980. Reinvestigation and application of olivine–quartz–orthopyroxene barometry. *Earth and Planetary Science Letters*, **47**, 1–10.

Carmignani, L., Ghezzo, C., Gosso, G., Lombardo, B., Meccheri, M., Montrasio, A., Pertusati, P.C. & Salvini, F. 1989. Geological map of the area between David and Mariner glaciers, Victoria Land, Antarctica. *Memorie della Società Geologica Italiana*, **33**, 77–97.

Carswell, D.A. 1980. Mantle derived lherzolite nodules associated with kimberlite, carbonatite and basalt magmatism: a review. *Lithos*, **13**, 121–138.

Davey, F.J. & Brancolini, G. 1997. The late Mesozoic and Cenozoic structural setting of the Ross Sea region. *Antarctic Research Series*, **68**, 119–138.

Donaldson, C.H. 1979. An experimental investigation of the delay in nucleation of olivine in mafic magmas. *Contribution to Mineralogy and Petrology*, **69**, 21–32.

Edgar, A.D. 1973. *Experimental petrology, basic principles and techniques*. Oxford: Clarendon Press, 217 pp.

Edgar, A.D., Green, D.H. & Hibberson, W.O. 1976. Experimental petrology of a highly potassic magma. *Journal of Petrology*, **17**, 339–356.

Eggler, D.H. 1974. Effect of CO_2 on the melting of peridotite. *Yearbook Carnegie Institution of Washington*, **73**, 215–224.

Eggler, D.H. 1978. The effect of CO_2 upon partial melting of peridotite in the system Na_2O–CaO–Al_2O_3–MgO–CO_2 at 35 kb with an analyses of melting in a peridotite-CO_2–H_2O system. *American Journal of Science*, **278**, 305–343.

Ellis, D.J. & Green, D.H. 1979. An experimental study of the effect of Ca upon garnet-clinopyroxene Fe–Mg exchange equilibria. *Contribution to Mineralogy and Petrology*, **71**, 13–22.

Forbes, W.C. & Flower, M.F.J. 1974. Phase relations of titan-phlogopite, $K_2Mg_4TiAl_2Si_6O_{20}(OH)_4$: a refractory phase in the upper mantle? *Earth and Planetary Science Letters*, **22**, 60–66.

Gamble, J.A. & Kyle, P.R. 1987. The origins of glass and amphibole in spinel-wehrlite xenoliths from Foster Crater, McMurdo Volcanic Group, Antarctica. *Contribution to Mineralogy and Petrology*, **111**, 283–298.

GAMBLE, J.A., MCGIBBON, F., KYLE, P.R., MENZIES, M.A. & KIRSCH, I. 1988. Metasomatised xenoliths from Foster Crater, Antarctica: implications for lithospheric structure and processes beneath the Transantarctic Mountain Front. *Journal of Petrology*, Special Lithosphere Issue, 109–138.

GERLACH, D.C. & GROVE, T.L. 1982. Petrology of Medicine Lake Highland volcanics: characterization of endmembers of magma mixing. *Contribution to Mineralogy and Petrology*, **80**, 147–159.

GHIORSO, M.S. & SACK, R.O. 1995. Chemical mass transfer in magmatic processes. IV. A revised and internally consistent thermodynamic model for the interpolation and extrapolation of liquid–solid equilibria in magmatic systems at elevated temperatures and pressures. *Contribution to Mineralogy and Petrology*, **119**, 197–212.

GHIORSO, M.S., HIRSCHMANN, M. & SACK, R.O. 1994. MELTS: software for thermodynamic modeling of magmatic systems. *EOS, Transactions American Geophysical Union*, **75**, 571–576.

GOLDICH, S.S., TREVES, S.B., SUHR, N.H. & STUCKLESS, J.S. 1975. Geochemistry of the Cenozoic volcanic rocks of Ross Island and vicinity, Antarctica. *Journal of Geology*, **83**, 415–435.

GREEN, T.H. 1977. Garnet in silicic liquids and its possible use as aP–T indicator. *Contribution to Mineralogy and Petrology*, **65**, 59–67.

GREEN, T.H. & RINGWOOD, A.E. 1968. Genesis of the calc–alkaline igneous rock suite. *Contribution to Mineralogy and Petrology*, **18**, 105–162.

GREEN, D.H., HIBBERSON, W.O. & JAQUES, A.L. 1979. Petrogenesis of mid-ocean basalts. *In* MCELHINNY, W.H., *ed. The Earth: its origin, structure and evolution.* London: Academic Press, 265–299.

HARRINGTON, H.J. 1958. Nomenclature of rock units in the Ross Sea Region, Antarctica. *Nature*, **182**, 290.

HERZBERG, C.T. & CHAPMAN, N.A. 1976. Clinopyroxene geothermometry of spinel lherzolites. *American Mineralogist*, **61**, 626–637.

HORNIG, I. & WÖRNER, G. 1991. Zirconolite-bearing ultra-potassic veins in a mantle-xenolith from Mt. Melbourne volcanic field, Victoria Land, Antarctica. *Contribution to Mineralogy and Petrology*, **106**, 355–366.

HORNIG, I., WÖRNER, G. & ZIPFEL, J. 1991. Lower crustal and mantle xenoliths from the Mt. Melbourne volcanic field, Northern Victoria Land, Antarctica. *Memorie della Società Geologica Italiana*, **46**, 337–352.

KYLE, P.R. & COLE, J.W. 1974. Structural control of volcanism in the McMurdo volcanic group, Antarctica. *Bulletin of Volcanology*, **38**, 16–25.

LECHLER, P.J. & DESILETS, M.O. 1987. A review of the use of loss on ignition as a measurement of total volatiles in whole-rock analysis. *Chemical Geology*, **63**, 341–344.

LLOYD, F.E., ARIMA, M. & EDGAR, A.D. 1985. Partial melting of a phlogopite–clinopyroxenite nodule from south-west Uganda: an experimental study bearing on the origin of highly potassic continental rift volcanics. *Contribution to Mineralogy and Petrology*, **91**, 321–329.

MAALØE, S. & JAKOBSSON, S.P. 1980. The P–T phase relations of a primary oceanite from the Reykjanes peninsula, Iceland. *Lithos*, **13**, 237–246.

MAALØE, S. & PETERSEN, T.S. 1976. Phase relations governing the derivation of alkaline basaltic magmas from primary magmas at high pressures. *Lithos*, **9**, 243–252.

MORIMOTO, N., FABRIES, J., FERGUSON, A.K., GINZBURG, I.V., ROSS, M., SEIFERT, F.A., ZUSSMAN, J., AOKI, K. & GOTTARDI, G. 1988. Nomenclature of pyroxenes. *Mineralogy and Petrology*, **39**, 55–76.

MÜLLER, P., SCHMIDT-THOMÉ, M., KREUZER, H., TESSENSOHN, F. & VETTER, U. 1991. Cenozoic peralkaline magmatism at the western margin of the Ross Sea, Antarctica. *Memorie della Società Geologica Italiana*, **46**, 315–336.

NIMIS, P. 1995. A clinopyroxene geobarometer for basaltic systems on crystal-structure modeling. *Contribution to Mineralogy and Petrology*, **121**, 115–125.

ORLANDO, A., ARMIENTI, P., CONTICELLI, S., VAGGELLI, G. & MANETTI, P. 1997. Petrologic investigations on the primitive Cainozoic lavas of Northern Victoria Land, Antarctica. *In* RICCI, C.A., *ed. The Antarctic region: geological evolution and processes.* Siena: Terra Antartica Publication, 523–530.

PATTISON, D.R.M. & NEWTON, R.C. 1989. Reversed experimental calibration of the garnet–clinopyroxene Fe–Mg exchange thermometer. *Contribution to Mineralogy and Petrology*, **101**, 87–103.

PERINELLI, C., ARMIENTI, P., TRIGILA, R. & AURISICCHIO, C. 1998. Intergranular melt inclusions within ultramafic xenoliths from Baker rocks and Green Point volcanics (Northern Victoria Land, Antarctica). *Terra Antarctica*, **5**, 217–233.

POLI, G., MANETTI, P., PECCERILLO, A. & CECCHI, A. 1977. Determinacione di alcuni elementi del gruppo delle terre rare in rocce silicatiche per attivacione neutronica. *Rendiconti della Società Italiana di Mineralogia e Petrologia*, **33**, 1061–1107.

RÅHEIM, A. & GREEN, D.H. 1974. Experimental determination of the temperature and pressure dependence of the Fe–Mg partition coefficient for coexisting garnet and clinopyroxene. *Contribution to Mineralogy and Petrology*, **48**, 179–203.

RAPP, R.P. & WATSON, E.B. 1995. Dehydration melting of metabasalt at 8–32 kbar: implications for continental growth and crust-mantle recycling. *Journal of Petrology*, **36**, 891–931.

RICKWOOD, P.C. 1968. On recasting analyses of garnet into end-member molecules. *Contribution to Mineralogy and Petrology*, **18**, 175–198.

ROEDER, P.L. & EMSLIE, R.F. 1970. Olivine-liquid equilibrium. *Contribution to Mineralogy and Petrology*, **29**, 275–289.

SALVINI, F., BRANCOLINI, G., BUSETTI, M., STROTI, F., MAZZARINI, F. & COREN, F. 1997. Cenozoic geodynamics of the Ross Sea Region, Antarctica: crustal extension, intraplate strike-slip faulting and tectonic inheritance. *Journal of Geophysical Research*, **102**, B11, 24 669–24 696.

STOLPER, E. 1980. A phase diagram for mid-ocean ridge basalts: preliminary results and implications for petrogenesis. *Contribution to Mineralogy and Petrology*, **74**, 13–28.

TONARINI, S., ROCCHI, S., ARMIENTI, P. & INNOCENTI, F. 1997. Constraints on timing of Ross Sea rifting inferred from Cainozoic intrusions from Northern Victoria Land, Antarctica. *In* RICCI, C.A., *ed. The Antarctic region: geologiucal evolution and processes.* Siena: Terra Antartica Publication, 511–522.

TREHU, A.M., HOLT, T., BEHRENDT, J.C. & FRITSCH, J. 1989. Crustal structure in the Ross Sea, Antarctica: preliminary results from GANOVEX V. *EOS, Transactions American Geophysical Union*, **70**, 1344.

VAGGELLI , G., OLMI, F. & CONTICELLI, S. 1999. Quantitative electron microprobe analysis of reference silicate mineral and glass samples. *Acta Vulcanologica*, in press.

WASS, S.Y. 1980. Geochemistry and origin of xenolith-bearing and related alkali basaltic rocks from the southern Highlands, New South Wales, Australia. *American Journal of Science*, **280A**, 639–666.

WASS, S.Y. & ROGERS, N.W. 1980. Mantle metasomatism – precursor to continental alkaline volcanism. *Geochimica et Cosmochimica Acta*, **44**, 1811–1823.

WHITE, A.J.R. 1964. Clinopyroxenes from eclogites and basic granulites. *American Mineralogist*, **49**, 883–888.

WYLLIE, P.J. & HUANG, W.L. 1976. Carbonation and melting reactions in the system $CaO–MgO–SiO_2–CO$ at mantle pressures with geophysical and petrological applications. *Contribution to Mineralogy and Petrology*, **54**, 79–107.

YODER, H.S. & KUSHIRO, I. 1969. Melting of a hydrous phase: phlogopite. *American Journal of Science*, **267A**, 558–582.